JOURNAL OF PROPULSION AND POWER
Vol. 17, No. 5, September–October 2001

Mechanisms and Prediction Methods for Fan Blade Stall Flutter

M. Vahdati* and A. I. Sayma†
Imperial College, London, England SW7 2BX, United Kingdom
J. G. Marshall‡
Rolls-Royce plc., Derby, England DE24 8BJ, United Kingdom
and
M. Imregun§
Imperial College, London, England SW7 2BX, United Kingdom

A first aim is to distinguish between two flutter regimes that are commonly referred to as stall flutter because of their occurrence between a raised working line and the stall boundary. The first one is of aeroacoustic origin, and it arises from a match between the acoustic impedance of the intake duct and the upstream pressure perturbation due to fan vibration. The second type is directly related to flow separation effects and shock properties. Further objectives are to describe several numerical prediction methods, to compare their relative computational requirements, and to establish their bounds of applicability to various flutter types. The unsteady flow is either a linearization about a viscous nonlinear steady-state flow for a given mode of vibration, or it is fully nonlinear. The prediction methods are classified according to the way they treat the unsteady flow. In all cases, the fluid mesh was moved during the unsteady flow computations to follow the structural motion. The performance of the methods was ranked for a rig fan blade for which measurements were available. It was found that, near the stall boundary, flutter boundary could only be captured with an adequate representation of the unsteady viscous effects. It was concluded that the shock had a stabilizing effect whereas the separation area behind it had a destabilizing effect.

Nomenclature

E = kinetic energy during one vibration cycle
F = modal force
Q = damping Q factor
t = time
v = modal velocity
δ = logarithmic decrement
η = aerodynamic damping

Introduction

IN turbomachinery applications, flutter is usually associated with fan blades, though other compressor and low-pressure turbine blades may also suffer from such instabilities. Although the need to avoid flutter to preserve fan integrity is obvious, note that flutter is increasingly becoming a limiting factor in developing improved-efficiency designs, especially when flexible, slender, and unshrouded blades are used. For the most part, fan flutter is observed in 1–6 forward-traveling nodal diameter assembly modes, the blades usually vibrating in their first flap (1F) mode.

A recent review of turbomachinery aeroelasticity by Marshall and Imregun[1] also includes an overview of computational fluid dynamics (CFD) methods for unsteady flows. Most early flutter investigations of industrial configurations treat the fluid and the structure as two distinct media, and two separate analyses are linked via the surface pressure, which is converted to a set of sinusoidal forces and moments acting on the blade.[2] The flutter stability is determined by the amount of positive or negative damping exhibited by the complex eigenvalues of the aeroelastic system. More advanced time-domain techniques employ a finite element representation for the structural part and reduce the mode shapes to a set of aerodynamic coordinates.[3] Although the governing equations are solved separately, the structural motion due to fluid forces at the current time step is used as a boundary condition to the fluid flow at the next time step and vice versa. There are no restrictions on the aerodynamic model that can be used, the only limitation being the available computing power. Such approaches allow the inclusion of most nonlinear effects, both of structural and aerodynamic origin, and the flutter behavior is deduced from convergent, limit-cycle, or divergent time histories of the blade's aeroelastic motion. With advances in computational methods and faster computing hardware, full-assembly models with time-accurate aerodynamics and blade flexibility are beginning to emerge. Chew et al.[4] used such an approach to predict the flutter of a 26-bladed fan assembly and compared their results with experimental data. A major conclusion from this work was that part-speed assembly mode flutter could be predicted using an essentially inviscid unsteady flow model, provided that the starting steady-state flow was computed on a fine viscous mesh and that the steady-state losses were extrapolated to the inviscid unsteady solution, the so-called inviscid plus loss model approach. The conclusion at the time was that stall flutter was driven by an inviscid mechanism. As will be discussed later, further research revealed that, in spite of the flutter onset being predicted with an inviscid method, the explanation for the underlying mechanism was incomplete.

In spite of extensive research work over the last 40 years, an accurate prediction of the flutter boundaries remains a challenging problem. In general terms, flutter modeling needs to capture both global characteristics and local detail. The former include suction surface boundary layer as well as the shock position and magnitude of the steady-state flow, whereas the latter requires the modeling of small local variations, such as marginally different leading-edge profiles and shock oscillation. To complicate matters further, flutter may occur near the working line (the so-called part-speed flutter bite) or near the stall boundary. Although the flow is significantly different in each case, both types are usually classified as stall flutter because they occur between the working line and the surge line. Although there are many other types of flutter,[5] not all are relevant to modern

Received 27 September 2000; revision received 2 April 2001; accepted for publication 6 April 2001.

*Research Fellow, Mechanical Engineering Department, Exhibition Road; m.vahdati@ic.ac.uk.
†Research Fellow, Mechanical Engineering Department, Exhibition Road; a.sayma@ic.ac.uk.
‡Team Leader, Fan Aero/Aeroelasticity, Trent Hall 2, First Floor (SinA-43); john.marshall@rolls-royce.com.
§Reader, Mechanical Engineering Department, Exhibition Road; m.imregun@ic.ac.uk.

aeroengine fan assemblies for large civil aircraft. Here we will focus on the so-called stall flutter instabilities that may occur on early development engines during rig tests. Although the basic instability depends, for the most part, on the unsteady flow features and the structural behavior of the fan blade, the flutter margin is usually associated with other factors such as blade mistuning, blade/disk attachment, flow distortions at the inlet, those caused by bleeds, pylon and outlet guide vane (OGV) effects, intake duct properties, and acoustic liners.

As mentioned earlier, the exact mechanism of stall flutter is still somewhat difficult to define because of the many ways in which it can occur. A variant, known as the flutter bite, manifests itself as a series of very sharp stability drops for very narrow part-speed ranges. As demonstrated by Vahdati et al.,[6] such behavior is due to an impedance match between the intake acoustics and the upstream pressure perturbations created by the vibration of the fan assembly in a given nodal diameter mode. Their work considered a complete fan assembly plus an intake duct (Fig. 1a), and, once the steady-state flow was captured using a fine viscous mesh, the unsteady flow analysis was conducted in an inviscid plus loss model fashion, though the blade vibration was included. A series of flutter analyses was conducted for the 60–80% speed range in 2% speed increments by considering two different intake duct geometries. A key result, reproduced in Fig. 1b, indicates that the relative flutter margin, defined with respect to some arbitrary damping value, is markedly different for each intake. Because the numerical model of the fan assembly and the aerodynamic conditions were kept the same, the difference in the flutter behavior was clearly linked to the intake duct properties. The exact mechanism was identified by examining the ratio of the unsteady pressures and axial velocities in the duct domain. It was also speculated that the acoustics of the downstream OGV domain could be contributing to the instability of higher nodal diameter modes.

Aeroacoustic flutter, which occurs near the working line when the flow remains almost fully attached, is distinctly different from the classical stall flutter, which occurs near the stall boundary and which is the main topic of this investigation. For isolated aerofoils, it is well established that pure bending modes are stable unless there is flow separation, or torsional coupling. The aerodynamic conditions giving rise to classical stall flutter in aeroengine fan assemblies tend to occur at part-speed raised working lines, where the incidence

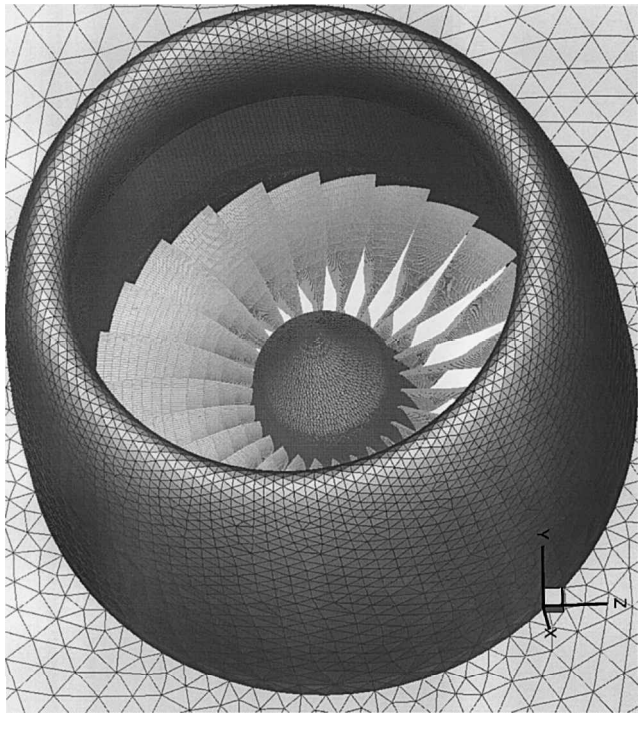

Fig. 1a Mesh for aeroacoustic fan flutter studies.

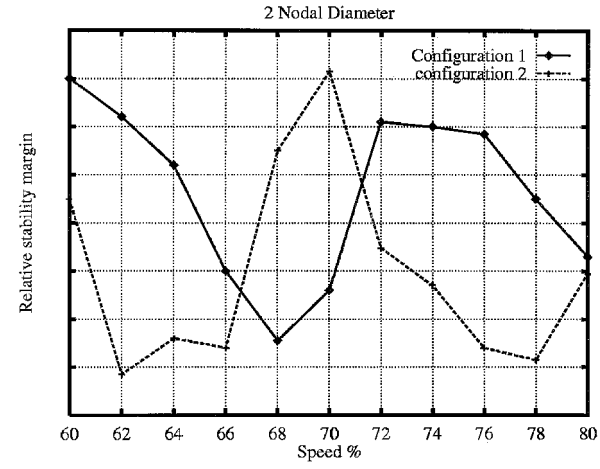

Fig. 1b Variation of flutter stability with speed for two different intake configurations.

onto the blades is high, a feature that results in thick boundary layers. For transonic flows, typical of front-stage fan blade tip sections at part speed, the shock is expelled from the passage (i.e., misses the leading edge of the next blade), and, hence, there is a strong shock/boundary-layer interaction. Features such as shock position, strength, and motion play an important role in the flutter mechanism and must be included in the analysis. One of the earliest stall flutter studies is reported by Sisto,[7] and review articles are presented by Chi and Srinivasan[8] and Ekaterinaris and Platzer.[9] Other detailed studies include the actuator disk analysis of Adamczyk et al.[10] and the composite wing of Dunn and Dugundji.[11] Because of the computational expense, most analyses are based on simplified models and usually ignore the unsteady viscous effects. In any case, when dealing with typical fan assembly geometries at representative aerodynamic conditions, a first major difficulty is the determination of the corresponding steady-state flowfield, a task that can be surprisingly difficult at part-speed transonic conditions with significant flow separation. As will be demonstrated later, the success of the classical stall flutter analysis is very much dependent on capturing the viscous features of the steady-state flow.

Overview of Stall Flutter Prediction Methodologies

Seven different three-dimensional flutter prediction methodologies will be considered in this paper. All methods model the unsteadiness due to the blade motion by using the same three-dimensional finite element model of the blade, though expanded assembly modes are used in whole-annulus analyses. Furthermore, all analyses use the same base steady-state viscous nonlinear flow with a Baldwin and Barth turbulence model and differ only in the way they treat the unsteady flow. Therefore, it is appropriate to classify the methods according to the unsteady flow modeling: 1) inviscid linearized,[12] 2) viscous linearized,[13] 3) single passage nonlinear inviscid flow with general interblade phase angle capability,[14] 4) as in the preceding, but including the loss model of Sayma et al.,[15] 5) as in the preceding, but replacing the loss model by a full viscous representation,[14] 6) whole-annulus nonlinear inviscid plus loss model unsteady flow,[4] and 7) as in the preceding, but replacing the loss model by a full viscous representation.[16]

With the exception of the inviscid linearized unsteady flow model, the CFD solver that is common to all other methods is based on unstructured meshes of tetrahedral, hexahedral, and wedge elements.[16] The blade geometry is discretized using an optimum semistructured mesh where the grid is unstructured in the blade-to-blade plane but structured in the radial direction.[17] The blade vibration is modeled at each time step by moving the aerodynamic mesh according to the structural motion. The surface unsteady pressures and displacements are exchanged as boundary conditions between the fluid and the structure.[18]

Broadly speaking, the ordering of the preceding list corresponds to the level of physical modeling and computational effort. The

linearized methods work in the frequency domain and assume small-amplitude harmonic vibration at fixed frequency and interblade phase angle (IBPA). The flutter stability is inferred from the (negative or positive) work done by the generalized aerodynamic force on the blade.

$$\text{work} = \int_{\text{period}} F v \, dt \tag{1}$$

where v is the modal velocity and F is the modal force. Negative work implies transfer of energy from the blade to the flow, and positive work done indicates a transfer of energy from the flow to the blade. The former case is stable, the latter case is unstable if the blade cannot dissipate the additional energy by some mechanical damping mechanism. When presenting the results, it is customary to quote aerodynamic damping in terms of logarithmic decrement (LOGDEC) values:

$$\delta = -\text{work}/2E \tag{2}$$

where E is the total kinetic energy during one period. The equivalent aerodynamic damping η and the aerodynamic Q factor may be obtained as

$$\eta = 1/Q = \delta/\pi \tag{3}$$

For a full flutter analysis, each IBPA of interest needs to be considered separately, though the analysis is often focused on low nodal diameter modes.

The ability to conduct a general IBPA flutter analysis using a nonlinear unsteady flow model on a single blade passage mesh is an attractive alternative to linearized methods because of the better modeling level it offers. However, the basic assumptions of prescribed IBPA and no modal coupling remain the same as before. The basic idea is to track the periodicity of the blade motion by storing the flow variables in time and to use these to impose a given IBPA.[19,20] The flutter solution procedure begins by prescribing a motion in a given nodal diameter mode by specifying the frequency and the vibration amplitude, which does not need to be small. The computation is continued until a periodic solution in time is obtained. As for linearized methods, the stability of the blade is determined from the work done by the fluid on the blade. Both methods ignore any frequency changes due to aerodynamic effects and can only analyze one mode at a time; thus, they cannot take into account any coupling between the modes. However, because the analysis is conducted for a single blade passage, the method has the advantage of being able to use fine meshes (for example, 500,000 points/passage), which makes it compatible with standard performance calculations. As such, single-passage flutter methods provide a very useful means of ranking the stability of successive blade designs.

Whole-annulus flutter calculations with a viscous unsteady time-accurate flow model are usually restricted to relatively coarse meshes because of computational limitations, though aeroelasticity calculations with over 15,000,000 points are becoming increasingly common.[21] Such analyses are conceptually the simplest because there are no built-in simplifying assumptions. The coupled fluid/structure calculation is initiated from some starting initial condition, and the flutter behavior is classified according to growing (unstable) or decaying (stable) blade motion. In spite of being computationally very expensive, whole-annulus flutter calculations have a number of important advantages:

1) All blade modes of interest, each leading to a family of assembly modes, can be included in the analysis. Such an approach not only allows modal interactions, but also yields the stability of all modes in a single consistent analysis.

2) The approach allows all aerodynamic instabilities to be considered simultaneously. For instance, if a particular operating condition is likely to cause rotating stall, the analysis will, in principle, indicate such behavior without any additional effort.

3) There are cases where the flutter stability is affected by the entire low-pressure compression system, including the intake, the OGVs, the pylons, and the bypass duct. Such cases can only be studied with a whole-annulus model because of the loss of symmetry: droop in the intake duct, nonsymmetric pylons, and nonuniformly staggered OGVs.

4) The flow stability of bird-damaged assemblies is becoming an increasingly important topic for engine certification purposes. Such numerical investigations, which are an attractive alternative to rig tests, can only be conducted with whole-annulus models.[22]

Case Study: Rig Fan Blade

A rig fan blade, typical of modern designs, was used as the benchmark geometry for assessing the performance of the preceding methods for the prediction of classical stall flutter. With the exception of the linearized inviscid method, the implementation of which is based on structured grids, semistructured blade meshes were used throughout the study.[17] As shown in Fig. 2, layers of unstructured mesh in the axial and tangential directions are connected in a structured fashion in the radial direction. The boundary-layer mesh was generated in a pseudostructured manner along the normals to the solid walls. Such a semiunstructured discretization produces a near-optimum distribution of the mesh points and allows the use of large numerical models with the available computational power. The grid contains about 330,000 points per passage, with 63 radial sections along the blade and 6 radial sections in the tip gap region. As will be discussed later, the tip gap was omitted from the whole-assembly calculations. The grid used for the inviscid flow analysis had only 20 radial sections and no boundary-layer mesh, resulting in 17,000 points per passage.

In rig tests, the flutter boundary is usually determined by following a given speed characteristic, and the same approach will also be adopted here with the numerical model. As shown in Fig. 3, eight different points, labeled 75c, 75a, 75d, 75e, 75e1, 75f, 75g, and 75h, were considered along the 75% speed line (the prefix 75 indicates the 75% speed characteristic). Converged steady-state solutions with Baldwin and Barth turbulence model were obtained for all eight cases by employing a mass-flow boundary condition where necessary. However, some numerical problems were encountered for the lowest mass-flow point, 75h, which is past the experimental flutter dip. The measured characteristic is also plotted in Fig. 3. Note that there are small differences between the individual points due to the way the aerodynamic boundary conditions were imposed.

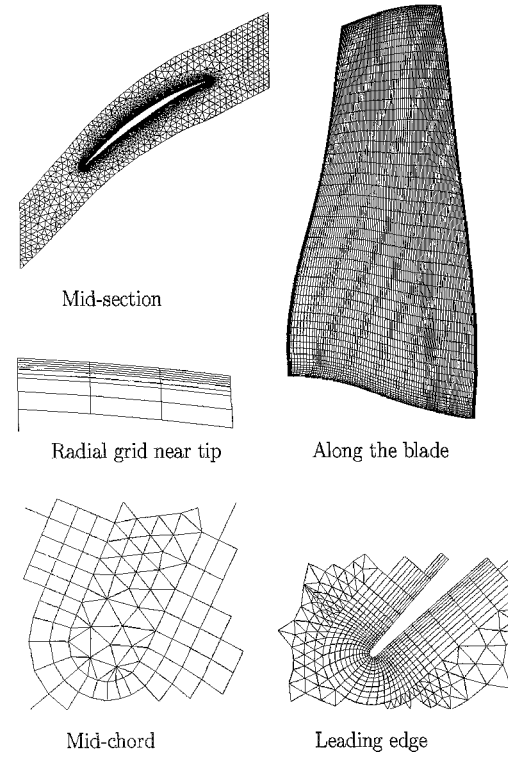

Fig. 2 Semistructured grid for single blade passage.

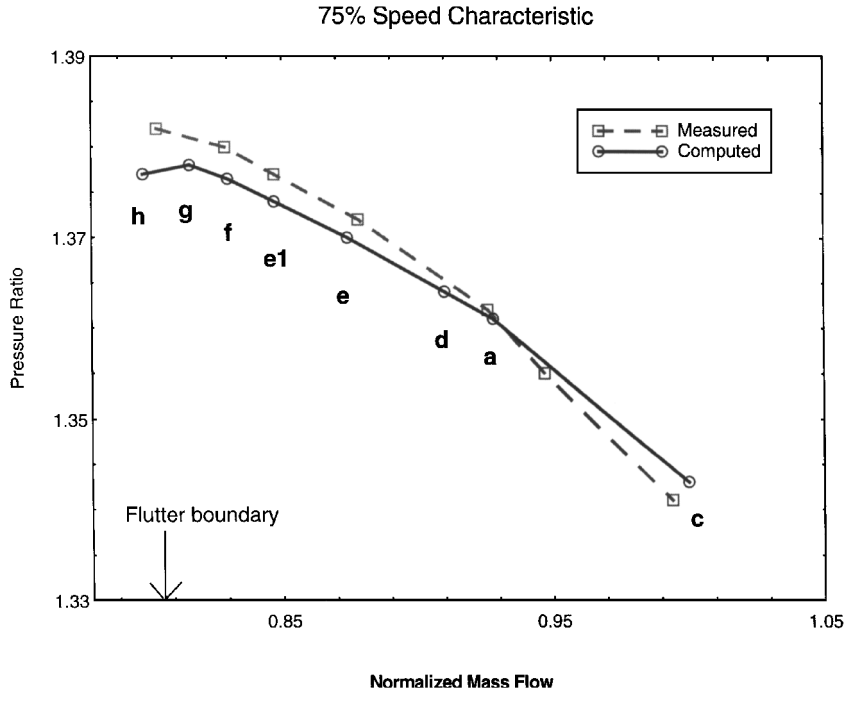

Fig. 3 Measured and predicted 75% speed characteristic for fan assembly.

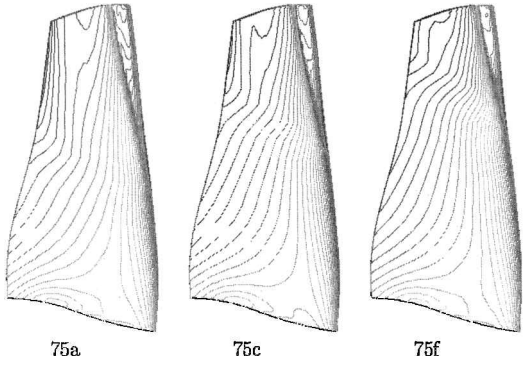

Fig. 4 Normalized steady-state pressure contours, suction surface.

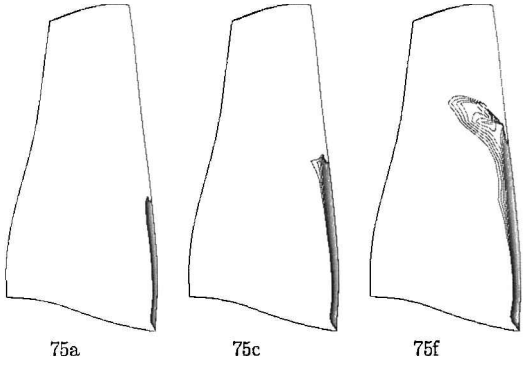

Fig. 5 Normalized negative axial velocity contours, suction surface.

The computed suction surface steady-state pressure profiles and the reverse flow, characterized by negative axial velocity obtained at the first point off the blade's surface, are shown in Figs. 4 and 5 for points 75a, 75c and 75f. The pressure profiles indicate that the shock moves slightly forward as the mass flow is decreased, but there are no significant differences between these three cases. However, an inspection of the negative axial velocity plots of Fig. 5 reveals a very distinct pattern: An increasing separated flow region is formed with decreasing mass flow.

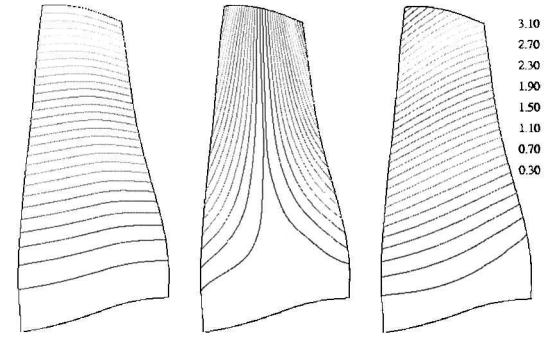

a) Bending component **b) Torsional component** **c) Actual mode shape**

Fig. 6 First flap mode shape for fan blade.

Flutter Calculations

We will now apply the seven flutter prediction methodologies of the preceding section to the case of a rig fan blade that is known to flutter along the 75% speed characteristic. Only one mode, namely, 1F, will be considered in the analysis. The actual mode shape is shown in Fig. 6c, and the bending and torsion components are plotted in Figs. 6a and 6b.

Single-Passage Nonlinear Viscous Analysis

To be able to track the periodicity of the blade motion, two layers of dummy points were created at the periodic boundaries. The flow variables were stored at the dummy points and then used to impose a given nodal diameter mode. The computation was continued until a periodic solution in time was obtained. The analysis was conducted for the 2, 3, and 4 nodal diameter assembly modes using a flow model both with and without a tip gap. Several points along the 75% characteristic were considered, and the results are summarized in Fig. 7. Note that there is a sharp decrease in the aerodynamic damping as the flow gets near the stall region. This flutter dip effect is predicted by both with- and without-tip-gap models, and the tip gap does not appear to have a major influence on flutter stability, at least for the particular case under study. For the purposes of predicting the flutter stability, the tip flow leakage effects are seen to be small compared to the overall viscous effects. The dominant

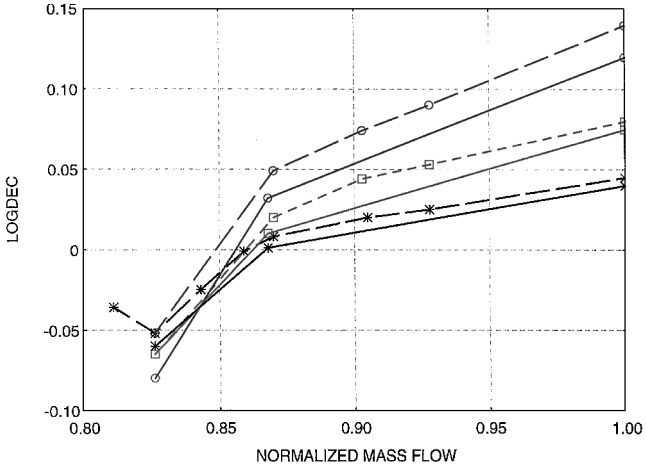

Fig. 7 Flutter stability via single-passage viscous computations: ——, with tip gap model; – – –, without tip gap model; ∗, 2ND mode; □, 3ND mode; and ○, 4ND mode.

flutter feature, the separated flow region of Figs. 4 and 5, is too far away from the tip region to be influenced directly. Furthermore, that the tip gap model yields less stable curves is consistent with increased unsteadiness due to tip leakage flows.

In any case, the minimum damping value occurs for a normalized mass-flow rate of about 0.827 and a further reduction in the mass flow does not reduce the aerodynamic damping any further. Even more surprisingly, there is flutter stability recovery for the 2 nodal diameter (2ND) mode as the stall boundary is approached farther. The significance of such a flutter dip will now be discussed further for the without-tip-gap case by considering the phase relationship between the aerodynamic excitation and the structural vibratory motion.

Figure 8a shows the 2ND modal force time history for points 75c and 75e for the last period of the converged solution. Also plotted in Fig. 8a is the modal velocity of the 1F mode. It is immediately seen that for the higher mass-flow points of 75c and 75e, the modal force is out of phase with the modal velocity, a feature that ensures positive aerodynamic damping. As the mass flow drops for points 75f and 75g of Fig. 8b, the modal force becomes in phase with the modal velocity, and, hence, the aerodynamic damping becomes negative, the so-called flutter point. Figure 9 shows the work done on the suction surface for points 75a, 75e, and 75f. Note that, as the mass flow drops between points 75a and 75f, the work done by the fluid on the blade increases. A comparison of Figs. 5 and 9 reveals that the (unstable) positive work region corresponds almost directly to the separated flow region. Such a correlation can be seen from Fig. 10, which shows the work done on the blade and 70% height as a function of the blade's chord. It is seen that the shock region is always very stable, whereas the area behind the shock is unstable, especially if the shock causes a separation of the boundary layer. Further calculations, not reported here, showed that work profiles at 70% blade height were three times higher than those at 90% height. This is because there is no separated flow at 90% height.

Single-Passage Nonlinear Inviscid Analysis With/Without a Loss Model

The analysis of the preceding section was repeated by replacing the unsteady viscous flow model with an inviscid one. As mentioned earlier, the computations were performed on a much coarser grid with 17,000 points per passage. Two types of calculations, with and without a loss model, were performed. In the first type, some of the viscous effects were retained by using a loss model that assumes that the unsteady losses can be approximated by their viscous steady-state counterparts. Steady-state viscous terms of the earlier fine mesh were extrapolated to the coarser mesh. The results are summarized in Fig. 11a, from which it is seen that the loss model computations are able to capture the flutter dip that was predicted by the earlier single-passage full viscous computations. However, the dip is now much smoother, indicating that the unsteady viscous effects play an

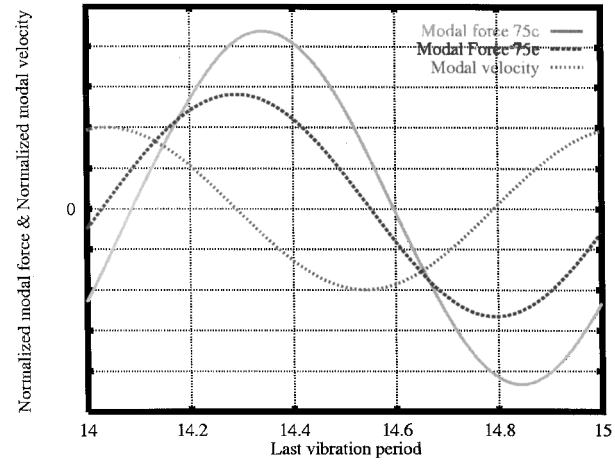

a) Modal force and modal velocity are out-of-phase for stable point 75f; phasing changes toward in-phase for less stable point 75e

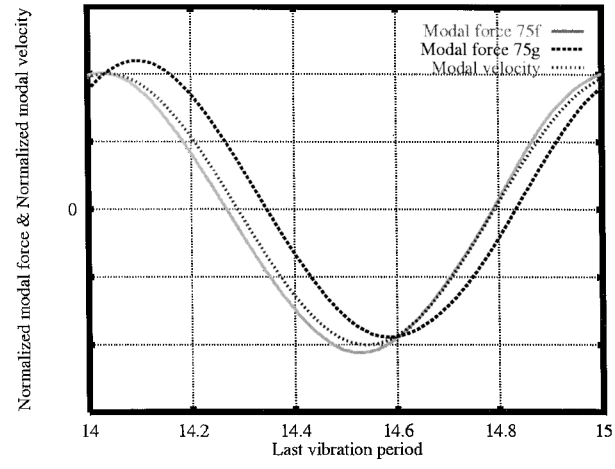

b) Modal force and modal velocity are in-phase for unstable point 75f; phasing changes toward out-of-phase for more stable point 75g

Fig. 8 Modal force and modal velocity plots for different points on 75% speed characteristic, 2ND mode, no tip gap.

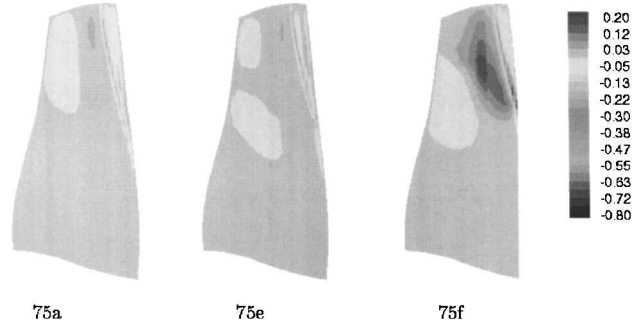

Fig. 9 Nondimensional work on suction surface.

important part in the mechanism of stall flutter. Further evidence is provided by the inviscid only calculations of Fig. 11b, which fail to detect the flutter instability at the correct mass-flow point. Although negative damping values are eventually predicted at much lower flow rates, such information is not particularly useful from a design viewpoint. A comparison of all flutter analyses will be given in Sec. 4.3 where this point will be discussed further.

Linearized Viscous Unsteady Analysis

As discussed by Sbardella and Imregun,[13] at least two options are available for linearizing the turbulent quantities: the so-called frozen eddy viscosity approach, where the mean-flow values are

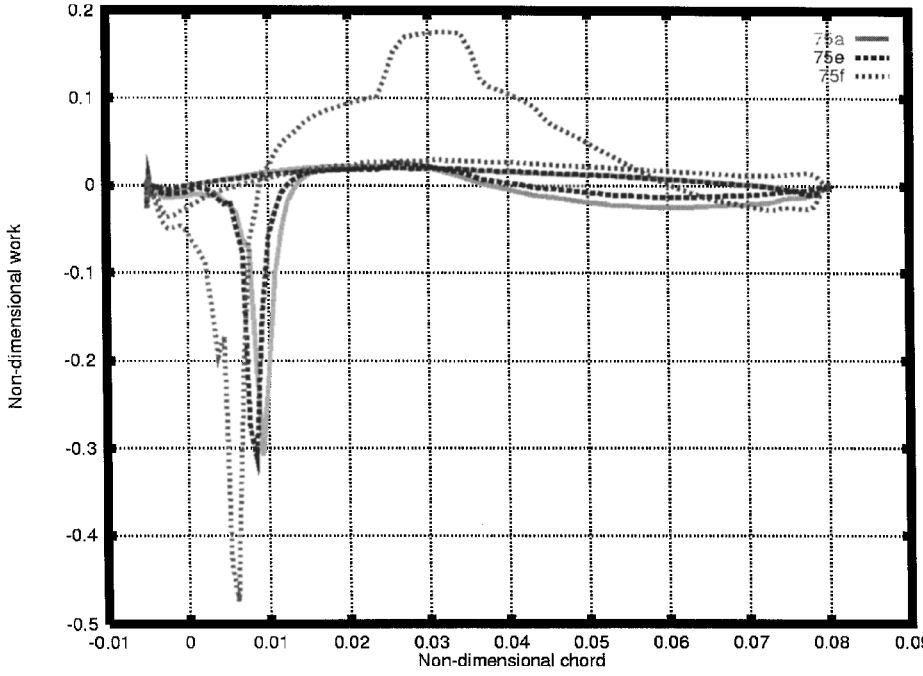

Fig. 10 Nondimensional work across chord for points 75a, 75e, and 75f.

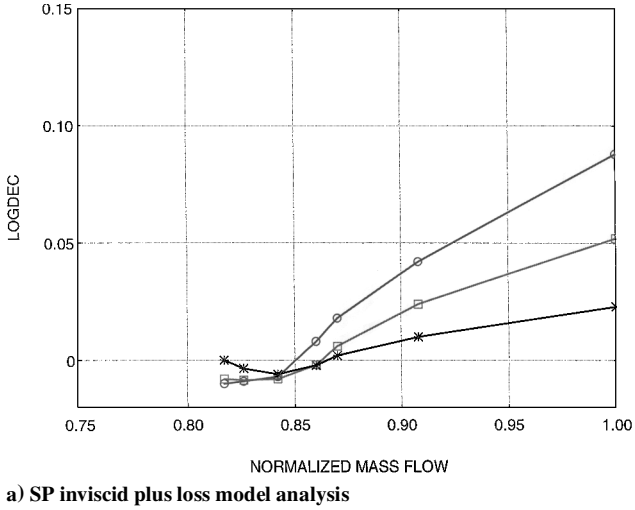

a) SP inviscid plus loss model analysis

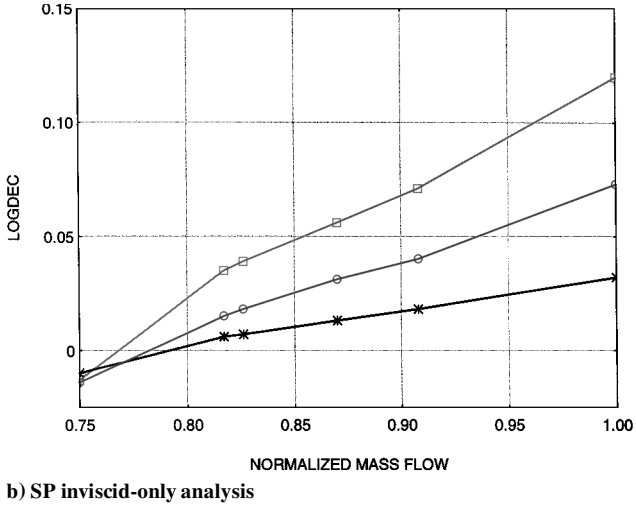

b) SP inviscid-only analysis

Fig. 11 Predicted flutter stability for 2, 3, and 4ND modes: ∗, 2ND mode; □, 3ND mode; and o, 4ND mode.

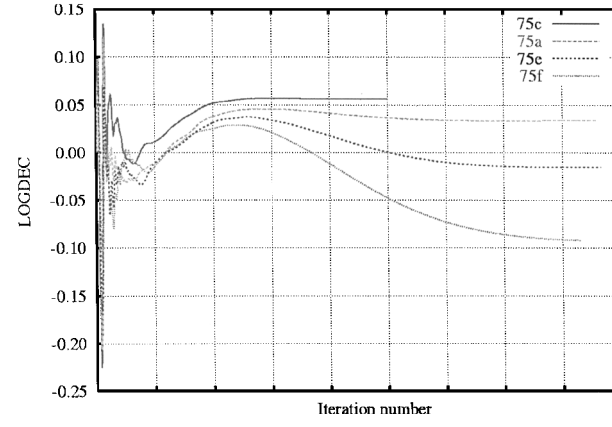

Fig. 12 LOGDEC convergence history for linearized viscous unsteady flow analysis.

used for the eddy viscosity, and the full linearization of the turbulence model. (The Spalart–Allmaras turbulence model was used in this study.) However, computational requirements will become significant when linearizing the viscous terms on fine boundary-layer meshes. The computations were, therefore, performed using the frozen eddy viscosity approach for the 2ND mode without a tip gap. Figure 12 shows the aerodynamic damping convergence time history for points 75a, 75c, 75e, and 75f. Note that the method is able to capture the drop in stability as the stall boundary is approached.

Whole-Assembly Nonlinear Unsteady Flow Analysis

The aim of this section is to compare the simplified single-passage analyses against a reference whole-assembly solution, both for viscous and inviscid unsteady flow modeling. In the viscous set of computations, the tip gap was omitted from the analysis because it was shown in Fig. 7 that it did not influence the flutter stability significantly. The starting steady-state solution and the grid used are shown in Fig. 13. The flutter analysis with a whole-annulus model starts by exciting all ND modes by applying an initial impulse to all of the blades. The stability of the assembly is then determined by tracking the individual modal time histories, which are either decaying (stable) or growing (unstable). Figures 14 and 15 show the comparison

Table 1 Overview of prediction methods

Method based on unsteady flow	Unsteady mesh/configuration	Modeling accuracy	Modal interaction	Normalized CPU hour/mode	Memory required	Suitability for design use
Inviscid linearized	50,000/SP[a] (structured mesh)	L[c]	No	10	L	L
Viscous linearized frozen Spalart–Allmaras	170,000/SP	H[e]	No	10	L	M
SP inviscid nonlinear loss model	17,000/SP	M[d]	No	1	L	H
SP viscous nonlinear Baldwin–Barth TM[f]	170,000/SP	H	No	20	L	H
Whole-assembly inviscid loss model	400,000/WA[b]	M	Yes	1	M	H
Whole-assembly viscous Baldwin–Barth TM	4,000,000/WA	H	Yes	10	H	M

[a]SP: single passage. [b]WA: whole assembly. [c]L: low. [d]M: medium. [e]H: high. [f]TM: turbulence model.

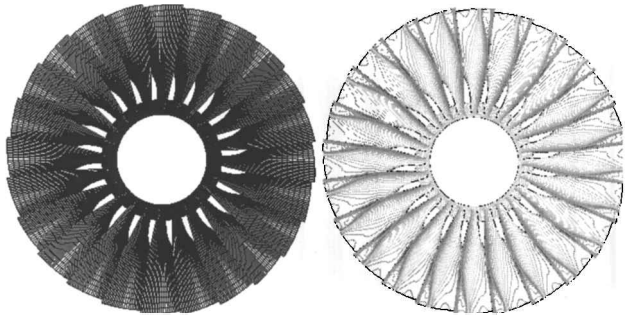

Fig. 13 Mesh and starting solution for whole-assembly analysis.

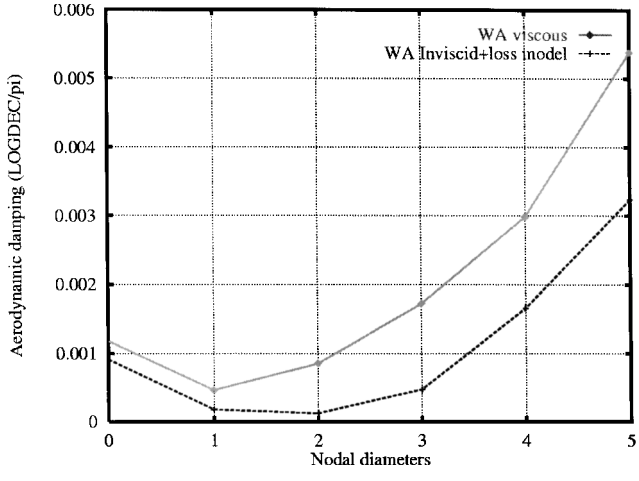

Fig. 14 Comparison of viscous and inviscid plus loss model flutter analyses, point 75a, whole assembly.

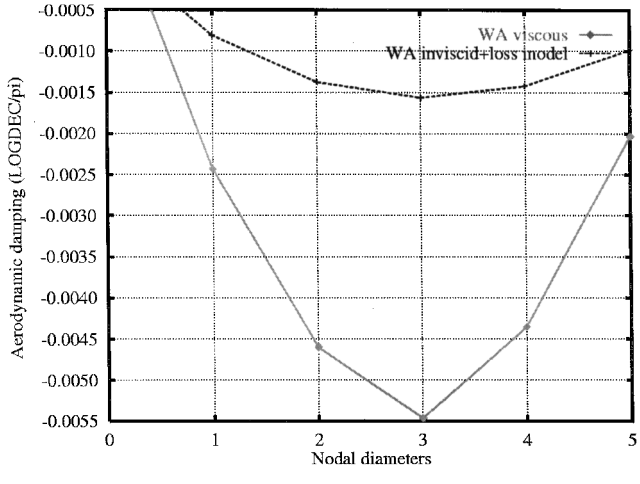

Fig. 15 Comparison of viscous and inviscid plus loss model flutter analyses, point 75f, whole assembly.

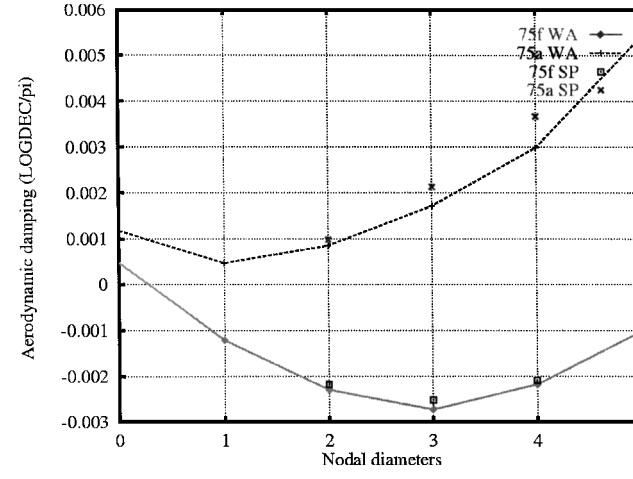

Fig. 16 Comparison of single-passage (SP) and whole-assembly (WA) analyses, viscous unsteady flow.

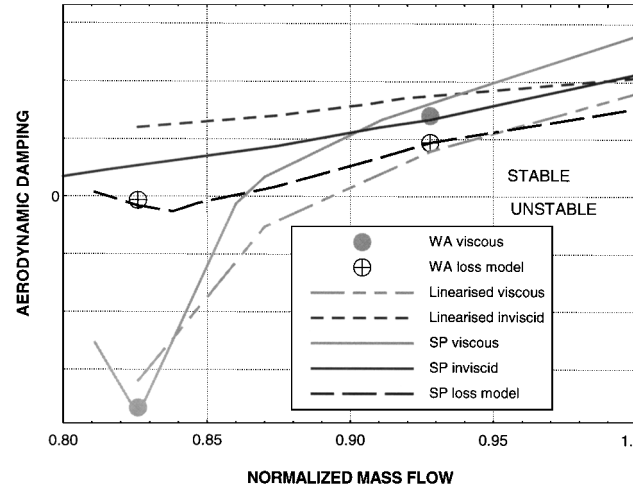

Fig. 17 Comparison of all flutter prediction methods for 2ND mode, classification by unsteady flow modeling: SP, single passage and WA, whole assembly.

of aerodynamic damping values between two whole-assembly flutter analyses, the first one using an inviscid plus loss model for the unsteady flow and the second using a full viscous representation. The relationship between aerodynamic damping and LOGDEC is given in Eq. (3). As can be seen from Fig. 14, the agreement between the two unsteady flow modeling levels is quite good for point 75a, which is near the working line. However, the second comparison, shown in Fig. 15 for point 75f, indicates that the stability is very much overpredicted by the loss model. In other words, the damping values from both methods are in agreement in the vicinity of the working line, but they are significantly different near stall boundary. Given that the mechanism of stall flutter is driven by viscous effects, such a finding is somewhat expected. Nevertheless, for the purposes of determining the flutter boundary, the inviscid plus loss model

representation appears to be adequate, though the prediction of the limit-cycle amplitude will require viscous unsteady flow modeling.

The single-passage and whole-assembly unsteady viscous flutter analyses are compared in Fig. 16, again for points 75a and 75f. Here the agreement is seen to be very good both at the working line and reasonable near the stall boundary, emphasizing the importance of viscous modeling and indicating that there are no significant modal interactions in this particular case for modes considered.

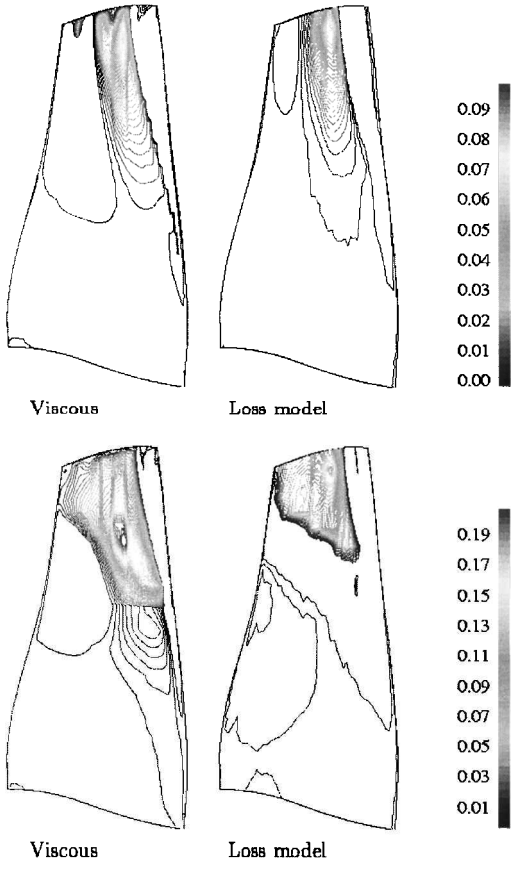

Fig. 18 Normalized positive (unstable) work-done plots from viscous and inviscid plus loss model flutter analyses: left, point 75c (near working line) and right, point 75f (near stall boundary).

Comparison of Flutter Results

Figure 17 shows a comparison of all flutter results so far for the 2ND mode, each damping vs mass-flow curve corresponding to a different modeling level. As mentioned earlier, with the exception of the linearized inviscid unsteady flow, all flutter computations were based on the same steady-state solution. As can be seen from Fig. 17, all methods appear to be in broad agreement near the working line. As the stall boundary is approached, there is a striking difference between the methods using viscous unsteady and inviscid unsteady flow models. Clearly, this feature can only be associated with the unsteady viscous effects becoming more important in flows with separated boundary layers. Consequently, only the viscous methods are able to predict the position of the flutter boundary correctly. For both nonlinear and linearized viscous computations, the flutter point, defined by the dip in the damping curve, is at a normalized flow rate of about 0.827, which is within 2.5% of the measured value of 0.808. Both the nonlinear and linearized inviscid calculations yield a straight damping vs mass-flow characteristic that totally misses the flutter point. If the linear decay continues, the flutter boundary will be predicted at unrealistically low mass-flow values. Finally, note that the results have been obtained for zero mechanical damping, the inclusion of which will move the flutter boundary to a slightly lower mass-flow rate, making the agreement even better. A summary of the flutter prediction methods, including the required computational effort, is given in Table 1.

Study of Stall Flutter Mechanism

The results so far indicate that viscous modeling is essential for the prediction of stall flutter, though the inviscid plus loss model approximation appears to be adequate in certain cases. The importance of retaining the viscous effects can be seen from the positive (unstable) work done plots of Fig. 18 for points 75c and 75f. The results were produced using the single passage nonlinear unsteady flow model. For point 75c (working line), the difference between the viscous model and the inviscid plus loss model is quite small, whereas there are major differences for point 75f (near stall boundary). Nevertheless, both modeling levels capture the trend, and, hence, flutter is predicted at about the correct mass flow. It is well known that flutter occurs in low-ND modes. A final calculation was made for point 75e to investigate the relative stability of the high-ND assembly modes. The work done on the suction surface is plotted in Fig. 19 as a function of the chord. Note that there is a gradual increase in stability with increasing ND numbers. The work done under the shock has a large stabilizing effect, especially for the 8ND mode.

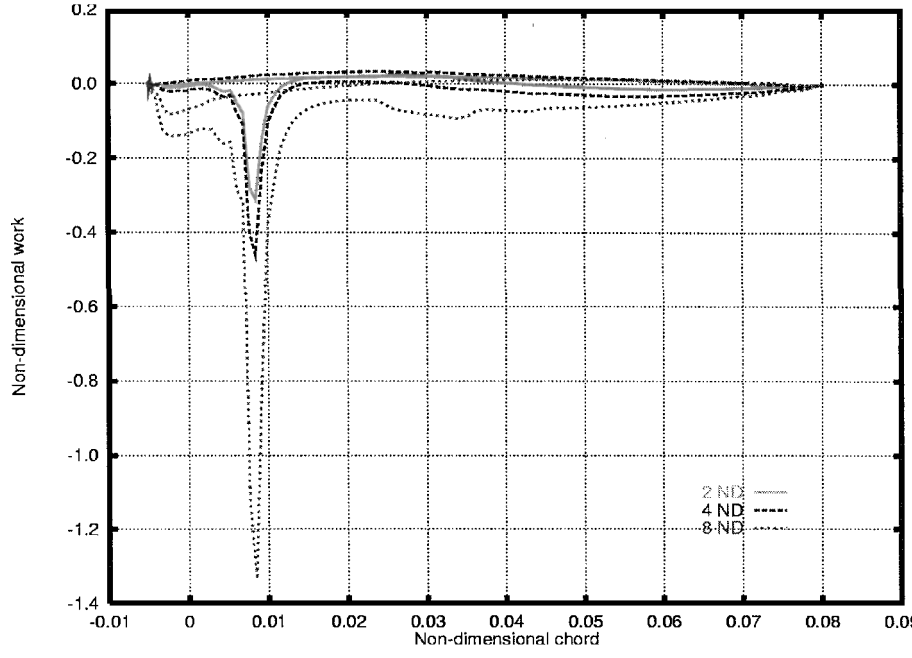

Fig. 19 Work done along blade's chord for 2, 4, and 8ND modes, 70% height.

Conclusions

1) One of the most critical requirements of a flutter analysis is the determination of the steady-state flow, a task that can be surprisingly difficult near the stall boundary. Turbulence modeling and the choice of imposed boundary conditions, namely, fixed pressure vs fixed mass flow, may play a crucial role for the convergence of the steady-state flow.

2) It appears that there are at least two mechanisms for part-speed stall flutter. The first one, aeroacoustic flutter, may occur very near the working line, and it is due to an impedance match between the intake duct acoustics and the upstream pressure perturbation created by the vibration of the fan assembly. As such, the viscous flow effects are probably of secondary importance, and inviscid unsteady flow representations may well be adequate. The second type, classical stall flutter, which is the main topic of this paper, occurs near the stall boundary, and viscous effects dominate its mechanism. For its prediction, one must use viscous flow representations, though inviscid plus loss model analyses are also able to capture the correct trend. However, inviscid linearization about a viscous steady-state solution is likely to introduce significant errors because of the removing/smoothing of the boundary layer.

3) The damping vs mass-flow characteristic is markedly nonlinear, a sudden drop, the so-called flutter dip, occurring at the flutter boundary. Further calculations, not reported here, indicate that the behavior is similar at other part speeds. This observation highlights the pitfalls of extrapolating aerodynamic damping values for lower mass-flow points from calculations at high mass-flow points.

4) For the particular case studied, only nonlinear and linearized viscous methods are able to capture the flutter dip. The inviscid plus loss model representation is also able to detect the flutter boundary, but the actual aerodynamic damping values are overestimated. The inviscid methods, nonlinear and linearized, fail to detect the flutter dip and yield a flat damping vs mass-flow rate characteristic.

5) For the particular case studied, whole-assembly and single-passage analyses produce very similar results, suggesting that modal interactions are negligible. Similarly, the effect of the tip gap on flutter stability seems to be small, though further geometries and flow conditions need to be studied before reaching firm conclusions.

6) From a computational viewpoint, the single-passage inviscid plus loss model approach appears to be attractive as a crude design tool. Better accuracy is provided by the linearized viscous analysis at 10 times the computational cost. Single-passage nonlinear viscous analysis is likely to be more accurate still, but the computational cost is double that of the linearized method.

7) From a design viewpoint, it may be possible to infer the flutter stability for similar blade designs from a careful inspection of the steady-state solution. The shock region always has a stabilizing effect, and the separation area behind the shock has a destabilizing effect.

Acknowledgments

The authors would like to thank Rolls-Royce plc. for both sponsoring this work and allowing its publication. They gratefully acknowledge the contribution of their colleagues at Rolls-Royce plc. (N. Cumpsty, C. Freeman, D. Halliwell, A. B. Parry, A. Rae, and N. Smith), at the Surrey University (J. W. Chew), and at Imperial College (C. Bréard and L. Sbardella).

References

[1]Marshall, J. G., and Imregun, M., "A Review of Aeroelasticity Methods with Emphasis on Turbomachinery Applications," *Journal of Fluids and Structures*, Vol. 10, No. 3, 1996, pp. 237–267.

[2]Kielb, R. E., and Ramsey, J. K., "Flutter of a Fan Blade in Supersonic Axial Flow," *Journal of Turbomachinery*, Vol. 111, No. 3, 1989, pp. 462–467.

[3]Guruswamy, G. P., and Goorjian, P. M., "Unsteady Transonic Aerodynamics and Aeroelastic Calculations at Low Supersonic Freestreams," *Journal of Aircraft*, Vol. 25, No. 10, 1988, pp. 955–961.

[4]Chew, J. W., Marshall, J. G., Vahdati, M., and Imregun, M., "Part-Speed Flutter Analysis of a Wide-Chord Fan Blade," *Unsteady Aerodynamics and Aeroelasticity of Turbomachines*, edited by T. H. Fransson, Kluwer Academic, Dordrecht, The Netherlands, 1998, pp. 707–724.

[5]Sisto, F., "Introduction and Overview," *AGARD Manual on Aeroelasticity in Axial-Flow Turbomachines, Unsteady Turbomachinery Aerodynamics*, NATO, AGARD-AG-297, Vol. 1, 1987, Chap. 1–13, pp. 1.1–1.13.

[6]Vahdati, M., Bréard, C., Sayma, A. I., and Imregun, M., "Computational Study of Intake Duct Effects on Fan Flutter Stability," *AIAA Journal* (to be published).

[7]Sisto, F., "Stall Flutter in Cascades," *Journal of the Aeronautical Sciences*, Vol. 20, No. 9, 1953, pp. 598–604.

[8]Chi, R. M., and Srinivasan, A. V., "Some Recent Advances in the Understanding and Prediction of Turbomachine Subsonic Stall Flutter," *Journal of Engineering for Gas Turbines and Power*, Vol. 107, No. 2, 1985, pp. 408–417.

[9]Ekaterinaris, J. A., and Platzer, M. F., "Progress in the Analysis of Blade Stall Flutter," *Unsteady Aerodynamics and Aeroelasticity of Turbomachines*, edited by Y. Tanida and M. Namba, Elsevier, Amsterdam, 1995, pp. 287–302.

[10]Adamczyk, J. J., Stevans, W., and Jutras, R., "Supersonic Stall Flutter of High-Speed Fans," *Journal of Engineering for Power*, Vol. 104, No. 3, 1982, pp. 675–682.

[11]Dunn, P., and Dugundji, J., "Nonlinear Stall Flutter and Divergence Analysis of Cantilevered Graphite Epoxy Wings," *AIAA Journal*, Vol. 30, No. 1, 1992, pp. 153–162.

[12]Marshall, J. G., and Giles, M. B., "Some Applications of a Time-Linearized Euler Method to Flutter and Forced Response in Turbomachinery," *Unsteady Aerodynamics and Aeroelasticity of Turbomachines*, edited by T. H. Fransson, Kluwer Academic, Dordrecht, The Netherlands, 1998, pp. 225–240.

[13]Sbardella, L., and Imregun, M., "Linearized Unsteady Viscous Turbomachinery Flows on Hybrid Grids," *Journal of Turbomachinery* (to be published).

[14]Sayma, A. I., and Vahdati, M., "Single Passage Non-Linear Unsteady Flow Models for Flutter and Forced Response," Imperial College Vibration Univ. Technology Centre Rept. VUTC/1/MM010, Imperial College, Mechanical Engineering Dept., London, 2000.

[15]Sayma, A. I., Vahdati, M., Green, J. S., and Imregun, M., "Whole-Assembly Flutter Analysis of a Low Pressure Turbine Blade," *Aeronautical Journal*, Vol. 43, No. 1, 1998, pp. 459–463.

[16]Sayma, A. I., Vahdati, M., Sbardella, L., and Imregun, M., "Modeling of Three-Dimensional Viscous Compressible Turbomachinery Flows Using Unstructured Hybrid Grids," *AIAA Journal*, Vol. 38, No. 6, 2000, pp. 945–954.

[17]Sbardella, L., Sayma, A. I., and Imregun, M., "Semi-Structured Meshes for Axial Turbomachinery Blades," *International Journal for Numerical Methods in Fluids*, Vol. 32, No. 5, 2000, pp. 569–584.

[18]Vahdati, M., and Imregun, M., "Non-Linear Integrated Aeroelasticity Analysis of a Fan Blade Using Unstructured Dynamic Meshes," *Journal of Mechanical Engineering Science, Part C*, Vol. 210, No. 5, 1996, pp. 549–563.

[19]Erdos, J. I., Alzner, E., and McNally, W., "Numerical Solution of Periodic Transonic Flow Through a Fan Stage," *AIAA Journal*, Vol. 15, No. 11, 1977, pp. 1559–1571.

[20]He, L., "Method of Simulating Unsteady Turbomachinery Flows with Multiple Perturbations," *AIAA Journal*, Vol. 30, No. 11, 1992, pp. 2730–2735.

[21]Sayma, A. I., Vahdati, M., Lee, S. J., and Imregun, M., "Forced Response Analysis of a Vertical Take-Off Liftfan in Aircraft Configuration," *Proceedings of the 6th National High Cycle Fatigue Conference*, Office of Naval Research, Naval Space Science and Tech. Program, March 2001.

[22]Imregun, M., and Vahdati, M., "Aeroelasticity Analysis of a Bird-Damaged Fan Assembly Using a Large Numerical Model," *Aeronautical Journal*, Vol. 103, No. 1030, 1999, pp. 569–578.